

Article

Promoted Performance of Layered Perovskite $\text{PrBaFe}_2\text{O}_{5+\delta}$ Cathode for Protonic Ceramic Fuel Cells by Zn Doping

Birkneh Sirak Teketel^{1,2,3}, Bayu Admasu Beshiwork^{1,3} , Dong Tian³, Shiyue Zhu³, Halefom G. Desta^{1,3}, Khan Kashif¹, Yonghong Chen³ and Bin Lin^{1,2,3,*}

- ¹ School of Mechanical and Electrical Engineering, School of Materials and Energy, University of Electronic Science and Technology of China, Chengdu 611731, China; siraku642@gmail.com (B.S.T.); admasu.beshiwork@aastu.edu.et (B.A.B.); halefomg2011@gmail.com (H.G.D.); kashif0101@yahoo.com (K.K.)
- ² Yangtze Delta Region Institute (Huzhou), University of Electronic Science and Technology of China, Huzhou 313001, China
- ³ Anhui Key Laboratory of Low-Temperature Co-Fired Material, Huainan Engineering Research Center for Fuel Cells, Huainan Normal University, Huainan 232001, China; tiandong111@163.com (D.T.); zhusy1@mail.ustc.edu.cn (S.Z.); chenyh@hnnu.edu.cn (Y.C.)
- * Correspondence: bin@uestc.edu.cn

Abstract: Proton-conducting solid-oxide fuel cell (H-SOFC) is an alternative promising low-temperature electrochemical cell for renewable energy, but the performance is insufficient because of the low activity of cathode materials at low temperatures. A layered perovskite oxide $\text{PrBaFe}_{1.9}\text{Zn}_{0.1}\text{O}_{5+\delta}$ (PBFZ) was synthesized and investigated as a promising cathode material for low-temperature H-SOFC. Here, the partial substitution of Fe by Zn further enhances the electrical conductivity and thermal compatibility of $\text{PrBaFe}_2\text{O}_{5+\delta}$ (PBF). The PBFZ exhibits improved conductivity in the air at intermediate temperatures and good chemical compatibility with electrolytes. The oxygen vacancy formed at the PBFZ lattice due to Zn doping enhances proton defects, resulting in an improved performance by extending the catalytic sites to the whole cathode area. A single cell with a Ni-BZCY anode, PBFZ cathode, and $\text{BaZr}_{0.7}\text{Ce}_{0.2}\text{Y}_{0.1}\text{O}_{3-\delta}$ (BZCY) electrolyte membrane was successfully fabricated and tested at 550–700 °C. The maximum power density and R_p were enhanced to 513 $\text{mW}\cdot\text{cm}^{-2}$ and 0.3 $\Omega\cdot\text{cm}^2$ at 700 °C, respectively, due to Zn doping.

Keywords: H-SOFC; layered perovskite; proton defect; Zn doping; double perovskite; oxygen vacancy



Citation: Teketel, B.S.; Beshiwork, B.A.; Tian, D.; Zhu, S.; Desta, H.G.; Kashif, K.; Chen, Y.; Lin, B. Promoted Performance of Layered Perovskite $\text{PrBaFe}_2\text{O}_{5+\delta}$ Cathode for Protonic Ceramic Fuel Cells by Zn Doping. *Catalysts* **2022**, *12*, 488. <https://doi.org/10.3390/catal12050488>

Academic Editors: Sabrina Campagna Zignani and José Joaquín Linares León

Received: 23 March 2022

Accepted: 15 April 2022

Published: 27 April 2022

Publisher's Note: MDPI stays neutral with regard to jurisdictional claims in published maps and institutional affiliations.



Copyright: © 2022 by the authors. Licensee MDPI, Basel, Switzerland. This article is an open access article distributed under the terms and conditions of the Creative Commons Attribution (CC BY) license (<https://creativecommons.org/licenses/by/4.0/>).

1. Introduction

Solid-oxide fuel cell (SOFC) is a well-known power source with promise as an alternative solution for current energy problems due to the low pollutant and extensive fuel flexibility [1–5]. Conventional SOFC mainly uses $(\text{Y}_2\text{O}_3)_{0.08}(\text{ZrO}_2)_{0.92}$ (YSZ) electrolyte, which requires a relatively high working temperature (800–1000 °C) to conduct and achieve exceptional performance [3,4]. However, the high working temperature condition initiates several adverse reactions leading to remarkable performance and stability problems [5–7]. Consequently, a proton-conducting solid-oxide fuel cell (H-SOFC) that can operate at low temperatures (below 700 °C) has been developed to address issues associated with traditional high-temperature SOFCs [7,8]. Conversely, the oxygen reduction reaction (ORR) catalytic activity decreases at low temperatures due to the high polarization resistance of the cathode [9,10]. As an H-SOFC cathode material, it is critical to have a triple conducting behavior involving the co-conduction of three participants at low temperatures [8,11,12]. In addition, an excellent triple-phase boundary (TPB) (the junction of two solid phases and gas phases), and good chemical and thermal stability are essential properties required by effective cathode materials [9–12].

Double perovskite oxide with A-site layered structure ($\text{LnBaM}_2\text{O}_{5+\delta}$; Ln = lanthanides, M = transition metals) has attracted research attention because of their kind structure in

the crystal lattice [13–16]. As shown in Figure 1d, these oxides possess stacking layers of [BaO]-[MO_x]-[LnO_δ]-[MO_x]-[BaO] contributing to two-dimensional oxygen diffusion through oxygen vacancy formed in the crystal lattice at the LnO_δ and MO_x layers [12,17,18]. Various series of layered double perovskites, such as PrBa_{0.5}Sr_{0.5}Co_{1.5}Fe_{0.5}O_{5+δ} [6], PrBaCo₂O_{5+δ} [15], PrBaFe₂O_{5+δ} [19], GdBaFeNiO_{5+δ} [20], PrBa_{0.5}Sr_{0.5}Co₂O_{5+δ} [21], and NdBaFe_{1.9}Nb_{0.1}O_{5+δ} [22], have been studied for moderate-temperature SOFC cathode materials. According to Grimaud and his colleagues, double perovskite-based cathodes have gained much attention. They show good electrochemical performance than simple perovskite-based cathodes due to their layered structure suite for bulk oxygen diffusion and triple conducting (TCO) behavior [15,18]. However, their performance of H-SOFCs was still not sound when they were used as a cathode for oxide ion-conducting solid-oxide fuel cells (O-SOFCs) [15,21]. Furthermore, most layered perovskite-based cathodes are centered on a conductive and catalytically active cobalt metal and suffer from its high thermal expansion coefficient [17]. As a result, it is necessary to find cobalt-free cathodes for H-SOFC [6,7,23].

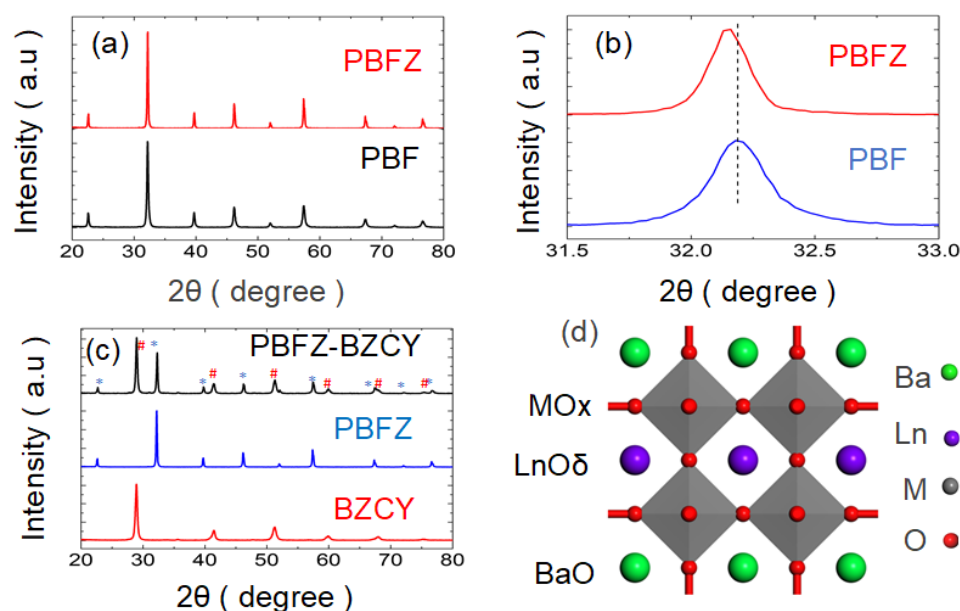


Figure 1. Crystal structure of PrBaFe_{1.9}Zn_{0.1}O_{5+δ} and its chemical compatibility with BZCY: (a) XRD patterns of PBFZ and PBF; (b) enlarged XRD pattern at a specific degree; (c) XRD patterns of PBFZ-BZCY mixed powders; (d) layered perovskite crystal structure.

Recently, iron-based layered perovskite has been studied for H-SOFC; Kim et al. discovered PrBaFe₂O_{5+δ} as a cathode for SOFC with a protonic electrolyte BaZr_{0.1}Ce_{0.7}Y_{0.2}O_{3-δ} (BZCY) and found a peak power density of 301 mW·cm⁻² at 700 °C [24]. Hanping et al. also reported PrBaFe₂O_{5+δ} (PBF) cathode for protonic SOFC using BaZr_{0.1}Ce_{0.7}Y_{0.1}Yb_{0.1}O_{3-δ} electrolyte and found a peak power density of 452 mW·cm⁻² [23]. (Pr, Ba)_{0.95}(Fe_{0.9}Mo_{0.1})₂O_{5+δ} was recently reported as a cathode for H-SOFCs and yielded an MPD of 532 mW·cm⁻² at 700 °C [25]. H. Ding and his colleagues have studied the consequence of Fe-doping on GdBaCoFeO_{5+δ} cathode and found a polarization resistance and maximum power density of 0.011 Ω·cm² and 482 mW·cm⁻², respectively, at 700 °C [26]. Accordingly, he concluded that Fe-doping increased the oxygen vacancies and improved single-cell electrochemical performance [26].

Though LnBaFe₂O_{5+δ} (Ln = lanthanides) based cathode materials are highly promising due to their high-temperature phase stability [18,23], they have lower electrochemical activity than Co-based materials due to their low conductivity and oxygen vacancies formation [27–29]. According to previous literature, Zn²⁺ doping significantly impacts oxygen vacancy concentration and affects proton, electron and oxide ions conduction, responsible for cell performance [27,30,31]. Zhen Hua et al. reported PrBaFe_{1.9}Zn_{0.1}O_{5+δ}

(PBFZ) based cathode for intermediate-temperature SOFC by substituting Fe by Zn^{2+} [13]. However, no proton conduction in PBFZ-based materials has been reported previously. This study proposed a layered PBFZ cathode for H-SOFCs with a spin-coated BZCY electrolyte and highlighted the consequence of Zn^{2+} doping on the performance of PBF based cathode material. In addition, the new proposed cathode's electrical conductivities (ECs), thermal expansion coefficients (TECs), and phase structure were all evaluated.

2. Results and Discussion

2.1. Crystal Structure and Chemical Compatibility

The X-Ray Diffraction (XRD) spectra of the PBFZ powder and its chemical compatibility with the BZCY electrolyte are provided in Figure 1. As seen in Figure 1a, there were no peaks attributed to impurities, and the peaks were well indexed as layered perovskite structure, reported previously [13,23]. PBFZ had a similar peak distribution to PBF powder without other additional phases (Figure 1a), indicating that Zn^{2+} was completely incorporated into the PBF lattice's B site. However, a small peak shifting to lower angle of diffraction was observed in PBFZ spectra due to the larger ionic size of Zn-ion ($Zn^{2+} = 0.74$) than Fe-ion ($Fe^{3+} = 0.65$, $Fe^{4+} = 0.59$) [13] (Figure 1b).

The XRD spectra of PBFZ-BZCY mixtures (50:50 wt.%) sintered at 1000 °C for 3 h were also presented to investigate the chemical reaction between them. As shown in Figure 1c, no new identifiable impurity peaks or XRD peak shifting were detected, indicating no apparent reaction between PBFZ and the electrolyte materials during cell operations at temperatures below 1000 °C.

2.2. Electrical Conductivity

The temperature-dependent electrical conductivity of PBF and PBFZ is shown in Figure 2. The conductivity of PBFZ increased with temperature and reached $3.5 \text{ S}\cdot\text{cm}^{-1}$ at 700 °C, confirming semiconducting behavior with a small polarons conduction mechanism [10,11,19]. At high temperatures (>700 °C), a metallic-like conduction behavior was observed, where conductivity decreased with temperature [10,19,32]. When the temperature increased beyond 700 °C, thermal reduction of the high valence state of Fe^{4+} to Fe^{3+} was accompanied by oxygen vacancy formation. This in turn decreased the concentration of charge carriers (electronic holes), resulting in decreasing conductivity [33,34]. As shown in Figure 2a, Zn-doped PBF had relatively better conductivity ($3.5 \text{ S}\cdot\text{cm}^{-1}$) than undoped PBF ($1.48 \text{ S}\cdot\text{cm}^{-1}$) at their respective high temperature (700 °C for PBFZ, 500 °C for PBF). When Zn was doping in the Fe-site of the $\text{PrBaFe}_2\text{O}_{5+\delta}$ crystal, the proportion of Fe^{4+} was increased to maintain the charge neutrality of the PBFZ and increase hole conduction, resulting in improved conductivity [35]. However, the conductivity was relatively low (see Figure 2) compared with the general required value of cathode materials ($100 \text{ S}\cdot\text{cm}^{-1}$) for SOFC [11,17], but the material had good performance. Similar phenomena were observed in previously reported electrode materials with low conductivity but high electrochemical performance [8,19,36].

The activation energies for both cathode material samples (PBFZ and PBF) were estimated from an Arrhenius-type plot and shown in Figure 2b. Two different curves for the PBFZ sample were formed due to different conductive rate nature [37]. The two curves were fitted by straight-line separately; at both high and low-temperature regions (Figure 2(b1,b2)). The conductive activation energy E_a values of the PBFZ sample were around 0.558 eV for the high-temperature area and 3.246 eV for the low-temperature region. At the same time, in PBF, a single fitting straight line was used, and the sample's conductive activation energy was 0.143 eV (Figure 2(b3)). The PBFZ sample showed more negative activation energy than the PBF sample; the number of charge carriers decreased faster with increasing temperature, resulting in a decrease in the conductivity rate with temperature increase [32,37,38].

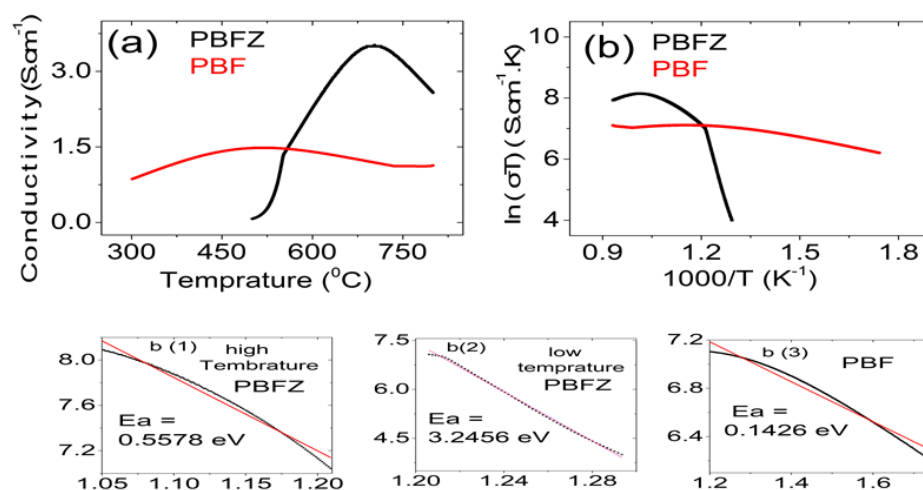


Figure 2. (a) Electrical conductivity of the PBFZ and PBF samples from 300 °C to 800 °C; (b) $\ln(\sigma T)$ vs. $1000/T$ (Arrhenius plot): (b(1),b(2)) fitting curves for PBFZ at different temperature range; (b(3)) fitting curve for PBF sample.

2.3. Thermal Expansion

Thermal expansion mismatch between cell components is the main challenge for developing long-term thermal cycling stable SOFC cells due to internal stress affecting the overall stability of cell operation [18,19,39,40]. Figure 3 shows the obtained thermal expansion curve of PBF and PBFZ samples tested from 20 °C to 800 °C in air. The curves were not linear throughout the temperature region; the value of dL/dL_0 increased at first with temperature and then exhibited a noticeable change in slope at around 400 °C. The change in the slope became smaller for PBFZ than PBF due to the constant di-valent oxidation state Zn^{2+} doping effect, which can alleviate the lattice expansion induced by the temperature [36,41]. The average thermal expansion coefficient (TEC) of PBF was $16.29 \times 10^{-6} K^{-1}$, while that of PBFZ was $12.98 \times 10^{-6} K^{-1}$ between 25 °C and 800 °C. The result shows that the TEC value was slightly affected by doping Zn into PBF and is comparable to previous research reported by Zhen Wang, et al. [36]. The calculated TEC values of both samples (PBFZ and PBF) tested below 800 °C are presented as a graph in Supplementary Materials (Figure S1).

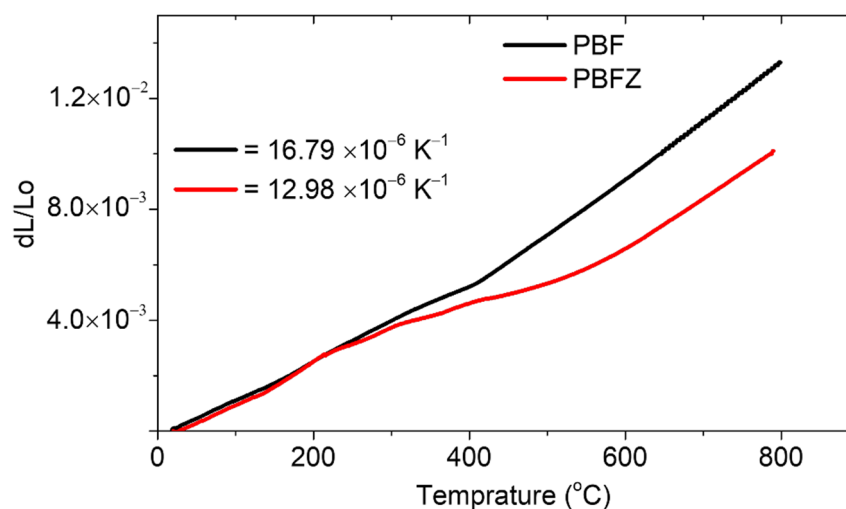


Figure 3. Thermal expansion curve of $PrBaFe_{1.9}Zn_{0.1}O_{5+\delta}$ and $PrBaFe_2O_{5+\delta}$ between room temperature and 800 °C.

The average calculated TEC value of PBFZ is obviously smaller and closer to BZCY ($10.1 \times 10^{-6} \text{ K}^{-1}$) [40] than that of cobalt-based double perovskite cathode materials such as $\text{PrBaFe}_2\text{O}_{5+\delta}$ ($18.7 \times 10^{-6} \text{ K}^{-1}$) [19], $\text{PrBaCoFeO}_{5+\delta}$ ($21.0 \times 10^{-6} \text{ K}^{-1}$) [42], and $\text{PrBaCo}_2\text{O}_{5+\delta}$ ($22.4 \times 10^{-6} \text{ K}^{-1}$) [43]. Due to unfavorable reduction of iron ion as cobalt ion, providing a lattice shrinkage results in a reduced and better thermal expansion match to the electrolyte [19,39,41]. When oxygen is lost from the lattice due to high temperatures [5,23], Fe^{4+} is reduced to Fe^{3+} , resulting in a high TEC due to the relatively large ionic radii of Fe^{3+} ($\text{Fe}^{3+} = 0.65$) compared to Fe^{4+} ($\text{Fe}^{4+} = 0.59$) [13,39]. Zn^{2+} doping in the PBF inhibits Fe^{4+} to Fe^{3+} reduction, reducing the amount of Fe^{3+} and lowering the value of TEC [30,41]. Therefore, Zn doping is an effective method for lowering the TECs of PBFZ, forming a good contact with the electrolyte, which is beneficial for the application of PCFCs. As a result, the possibility of electrolyte–cathode interface delamination during the high-temperature heating-cooling cycle is reduced.

2.4. ORR Activity

A symmetric cell was fabricated and measured its resistance change to estimate the potential of PBFZ as a cathode catalyst for ORR activity. Figure 4a shows the EIS plots of the PBFZ | $\text{Sm}_{0.1}\text{Ce}_{0.9}\text{O}_{2-\delta}$ (SDC) | PBFZ cell measured between 550 °C and 700 °C and fitted with an equivalent circuit model (L-Ro-(R₁Q)-(R₂Q)). The polarization resistance of PBF and PBFZ ($R_p = R_1 + R_2$) is an essential parameter of the cathode's activity during oxygen reduction reaction (ORR).

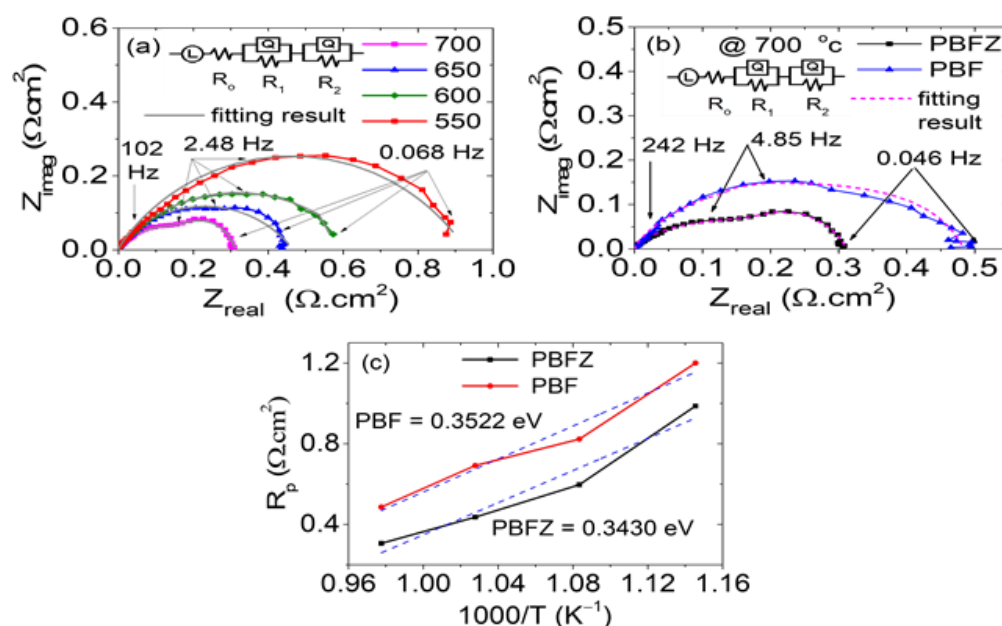


Figure 4. Nyquist plots of the symmetric cell (a) PBFZ | SDC | PBFZ, (b) PBFZ | SDC | PBFZ and PBF | SDC | PBF at 700 °C, (c) R_p values for PBFZ and PBF cathode from Arrhenius plots.

The EIS plots of PBF and PBFZ based symmetrical cells at 700 °C are presented in (Figure 4b). Based on the figure, the R_p values of PBFZ and PBF are $0.306 \Omega \cdot \text{cm}^2$ and $0.486 \Omega \cdot \text{cm}^2$, respectively at 700 °C (Figure 4b). As can be seen, the R_p value gradually decreases by approximately 37%, at 700 °C after Zn doping which is closely related to the formation of holes (Fe^{4+}) and oxygen vacancy in the PBFZ cathode [13]. To some extent, the doping of Zn^{2+} increases both the oxygen vacancy and formation of Fe^{4+} cations, which control the hole transport and oxygen ion diffusion kinetics, facilitating ORR activity and lowering R_p [8,27,31]. Furthermore, the minimum energy required to precede the ORR process (activation energy) was reduced from 0.3522 eV to 0.3430 eV due to Zn^{2+} doping (Figure 4c), confirming the ORR process's energy-efficient catalytic activity [27]. From

this standpoint, one could anticipate that Zn doping could significantly improve electrocatalytic activity by providing enough oxygen vacancy for efficient proton migration; a critical property of materials used as cathodes in H-SOFC.

2.5. Single-Cell Performance

The performance of PBFZ cathode for ORR in proton-conducting solid-oxide fuel cells was probed with the anode-supported single cell using H₂ fuel (3% H₂O) and air as an oxidant. Figure 5a shows I-V and I-P curves of PBFZ cathode-based cells from 550 °C to 700 °C. A comparative performance bar graph is presented in Figure 5b to compare the performance of cathodes at different temperatures. As shown in the figure, for PBFZ cathode, maximum power density (MPD) of 208 mW·cm⁻², 315 mW·cm⁻², 432 mW·cm⁻², and 513 mW·cm⁻² was obtained at 550 °C, 600 °C, 650 °C, and 700 °C, respectively. For PBF cathode, the MPDs are 102 mW·cm⁻², 169 mW·cm⁻², 257 mW·cm⁻², and 313 mW·cm⁻² at the same respective operating temperatures (Figure 5b and Figure S3).

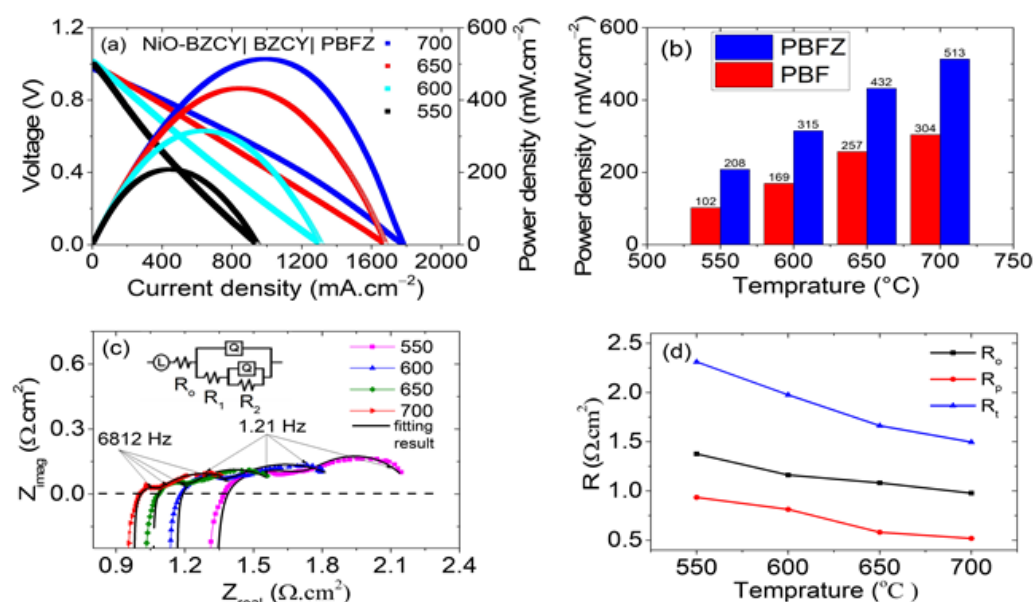


Figure 5. (a) I-V and I-P curves of single cells; (b) cell performance histogram; (c) impedance spectra of NiO-BZCY|BZCY|PBFZ; (d) Ohmic (R_o) polarization (R_p), and total (R_t) resistance of single-cell at different temperature.

As clearly stated, Zn-doped cathode has better MPDs than undoped one, which is consistent with previous studies [13,30,41]. This noticeable performance improvement is primarily due to the PBFZ's electrocatalytic activity than the undoped PBF cathode. It is noted that Zn doping results in oxygen vacancy formation, promoting proton uptake and mobility, resulting in better proton conduction [31,36,41]. When compared to other non-Co-based cathodes for H-SOFC, such as GdBaFeNiO_{5+δ} [20], LaBaCuFeO_{5+δ} [44], and NdBaFe_{1.9}Nb_{0.1}O_{5+δ} [22], PBFZ has a slightly higher peak power density at 700 °C. Moreover, the PBFZ cathode has better and comparable performance compared with some Co-based double perovskites such as (mostly active cathodes) listed in Table 1.

Table 1. Lists of peak power densities (PPDs) for previously reported proton-conducting SOFC using layered double perovskite as a cathode at 700 °C.

Cathode	Electrolyte	Thickness (μm)	MPD (mW·cm ⁻²)	Reference
SmBa _{0.5} Sr _{0.5} Co ₂ O _{5+δ}	BZCY	15	533	[16]
PrBaCo ₂ O _{5+δ}	BZCY	25	545	[17]
NdBaFe _{1.9} Nb _{0.1} O _{5+δ}	BZCY	30	392	[22]
(PrBa) _{0.95} (Fe _{0.9} Mo _{0.1}) ₂ O _{5+δ}	BZCY	25	359	[25]
PrBaCo ₂ O _{5+δ}	BZCYYb	15	490	[29]
LaBaCuFeO _{5+δ}	BZCY	20	327	[44]
NdBaCo ₂ O _{5+δ}	BZCY	10	438	[45]
PrBaF _{1.9} Zn _{0.1} O _{5+δ}	BZCY	30	513	This work
PrBaFe ₂ O _{5+δ}	BZCY	33	304	This work

Note: BZCY = BaZr_{0.1}Ce_{0.7}Y_{0.2}O_{3-δ}, BZCYYb = BaZr_{0.1}Ce_{0.7}Y_{0.1}Yb_{0.1}O_{3-δ}, MPD = Maximum peak power density.

The cell's resistance was tested under open-circuit condition and plotted as electronic spectra in Figure 5c. The polarization resistance (R_p) values (the sum of R_1 and R_2 in an equivalent circuit) of PBFZ based cell were reduced with the temperature increases, and the measured R_p value of the cell was 0.518 $\Omega\cdot\text{cm}^2$ at 700 °C (Figure 5d), which was smaller than 0.97 $\Omega\cdot\text{cm}^2$ of the PBF based cell at 700 °C (Figure S4). Compared to the high conductive cobalt-containing cathodes, such as NdBaCo₂O_{5+δ} (0.16 $\Omega\cdot\text{cm}^2$) [45] and PrBaCo₂O_{5+δ} (0.15 $\Omega\cdot\text{cm}^2$) [17], the R_p of PBFZ was much higher at or below 700 °C. The relationship between total resistance (R_t), polarization resistance, and ohmic resistance (R_o) is depicted in Figure 5d. R_p and R_o decrease slightly with increasing temperature. The value of R_p is less than R_o throughout the operating temperature, indicating that the ohmic resistance dominates the total cell resistance, implying that oxygen ion migration and diffusion in the electrolyte bulk were rate-determining steps in all cell processes [16,25].

2.6. Stability and Microstructure

Figure 6a shows the scanning electron microscope (SEM) micrographs of a single cell with a view of the anode, cathode, and electrolyte interfacial regions. The 30 μm thick electrolyte adhered well to the porous PBFZ cathode layers without delamination or fracture, implying that the cell has good charge transferability and stability [39]. The PBF based cell also had a well-dense electrolyte membrane about 33 μm thick and well stuck to the cathode and anode substrate (Figure S5a), but it was not as well attached to the BZCY electrolyte as PBFZ. Cracks and pores were found at the interface of the cathode and BZCY electrolyte in the case of the PBF based cell (Figure S5), which might be due to the much higher TEC value of PBF as previously discussed (Section 2.3). Based on SEM micrographs (Figure 6b), the porosity and particle size were uniformly distributed in the cathode, which allows for more diffusion paths and absorption sites. The relatively better microstructure observed in the PBFZ compared with the PBF cathode (Figure S5) could be the reason for the better performance obtained in this H-SOFC. Figure 6c shows the results of a short-term study of a PBFZ based single-cell tested for 720 min at 600 °C using moisture hydrogen (3% H₂O) as a fuel. The results indicate that the PBFZ cathode can operate continuously for 12 h without significant degradation, as evidenced by the cell's current density confirming a promising cathode material for H-SOFC.

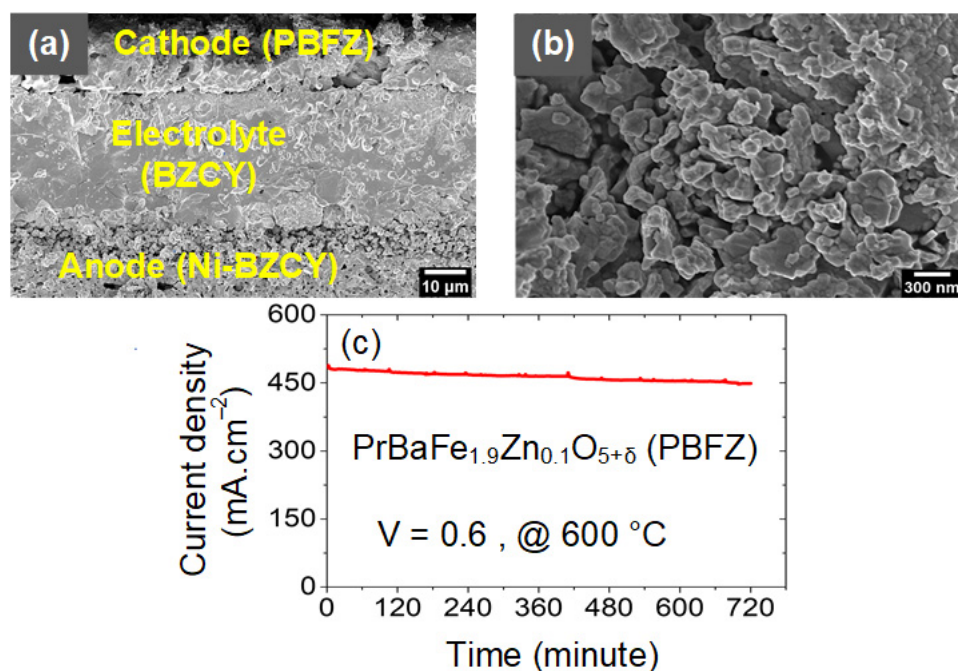


Figure 6. Short-term performance stability and microstructure: (a) SEM micrograph of NiO-BZCY/BZCY/PBFZ single-cell; (b) SEM micrographs of PBFZ cathode; (c) I-T curves with 0.6 V of a single cell at 600 °C.

The elemental distribution and composition of the PBFZ sample were investigated using an Energy dispersive X-ray Spectroscopy (EDX) equipped SEM. As shown in Figure 7, the elements of Pr, Ba, Fe, and Zn were uniformly distributed throughout, without phase segregation. The energy dispersive spectrum as well as the weight and atomic percentage of each constituent element of the cathodes sample are presented in the supporting information (Figure S6).

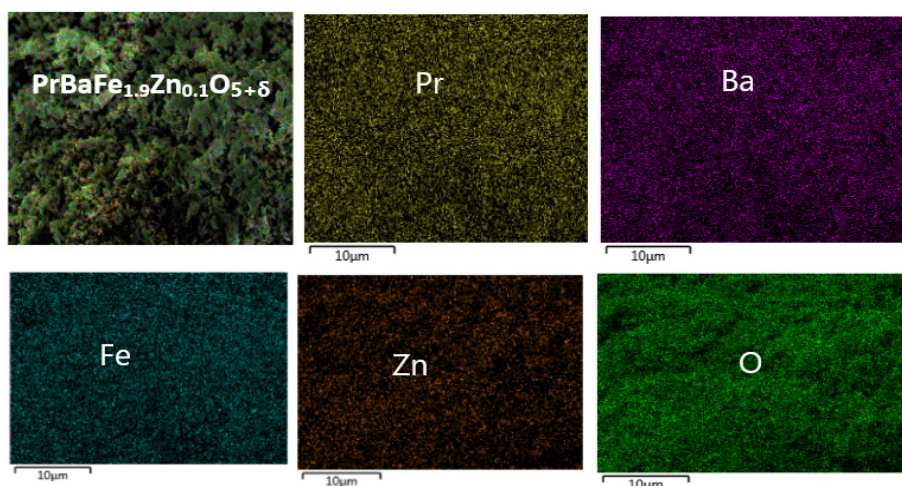


Figure 7. Elemental composition and distribution of PBFZ studied by EDX.

3. Materials and Methods

3.1. Material Synthesis and Characterization

The $\text{PrBaFe}_{1.9}\text{Zn}_{0.1}\text{O}_{5+\delta}$ and $\text{PrBaFe}_2\text{O}_{5+\delta}$ powders were prepared via the self-ignition combustion method [20]. A stoichiometric amount of starting precursors (metal nitrates); $\text{Pr}(\text{NO}_3)_3 \cdot 6\text{H}_2\text{O}$ (99.9%), $\text{Ba}(\text{NO}_3)_2$ (99.5%), $\text{Fe}(\text{NO}_3)_3 \cdot 9\text{H}_2\text{O}$ (98.5%), and $\text{Zn}(\text{NO}_3)_2 \cdot 6\text{H}_2\text{O}$ (99.5%) were added in deionized water followed by adding citric acid (CA) into the solution

at a molar ratio of 1.5 to metals. The solution's pH was adjusted to around 7–8 using ammonia solution and heated to form grey ashes. Finally, the powder was calcined at 1000 °C for 3 h to form a single-phase structure. BZCY and NiO powders were also prepared by the same method described above. The PBFZ's and PBF's powder crystal structure and their compatibility with BZCY electrolyte were determined by powder XRD (DX2800, Dandong Haoyuan Instrument Co. Ltd., Dandong, China) with Cu-K α radiation. The PBFZ's chemical compatibility with BZCY electrolyte was tested by XRD analysis of mixed powder (mixture of PBFZ and BZCY in 50:50 wt.% ratio) to determine whether there had been any other problems changes in phase composition due to the heat treatment. The thermal expansion curve of PBFZ and PBF was tested between 40 °C and 800 °C in the air using a dilatometer (NETZSCH-DIL-402C, Netzsch-Geratebau GmbH, selb, Germany). The test was done on a rectangular bar (20 × 5 × 2.5 mm) after sintering at 1100 °C for 4 h. A four-probe DC technique was applied to test the electrical conductivity of a dense rectangular bar (2.5 × 3.5 × 7.5 mm) of samples sintering at 1300 °C for 4 h. The measurements were performed in the air using a source meter (Keithley 2400, Tektronix, Cincinnati, USA) [31]. SEM (FE-SEM (Gemini SEM 300, Carl Zeiss, Jena, Germany) was used to check the morphology and microstructure of cells after the test.

3.2. Fabrication of Symmetrical and Single Cell

The spin-coating method was used to prepare a single cell with a thin electrolyte coated on the anode support [17,20]. The support was designed by pressing the ball-milled powder mixture (NiO:BZCY:starch = 60:40:20 wt.%) into a circular pellet. After sintering the support layer at 1100 °C for 3 h, the electrolyte slurry was spine coated on the anode support layer and co-fired again at 1400 °C for 5 h. Finally, the cathode slurry was brush painted onto the electrolyte surfaces of NiO-BZCY anode support and fired for 3 h at 1000 °C. The area of the painted cathode surface was 0.2 cm². The cathode's ORR activity (PrBaFe₂O_{5+ δ} and PrBaFe_{1.9}Zn_{0.1}O_{5+ δ}) was studied using a symmetrical configuration cell.

3.3. Electrochemical Performance and Impedance Test

The Electrochemical Impedance spectra (EIS) of symmetrical cell was tested from 700 °C to 550 °C using Zahner, IM6 (Zahner-Elektrik GmbH & Co.KG, kronach, Germany) workstation over a frequency range of 10 mHz-1 MHz. The output performances of NiO-BZCY/BZCY/PBFZ based single cells were also measured using the same workstation from 700 °C to 550 °C. The measurement was performed by sealing the single cell on the alumina tube using a ceramic glue sealant material and passing a moisture H₂ (3% H₂O) to the anode side as fuel. The single cell's current–voltage (I–V) curve was plotted between temperature ranges of 550 °C to 700 °C. The cell's impedance also measured at an open-circuit voltage (OCV) from 1 MHz to 0.01 Hz frequency range at 10 mV.

4. Conclusions

A layered perovskite oxide PBFZ has been devised as a cathode for H-SOFC with BZCY electrolyte. Detailed characterization and measurement have been done to probe the impact of Zn doping on catalytic activity, conductivity, thermal compatibility, and performance of PBFZ-based cells. The results have revealed that the electrical conductivity increased while the TEC decreased to $12.98 \times 10^{-6} \text{ K}^{-1}$ due to Zn doping. At 700 °C, the cell performance with PBFZ cathode and BZCY electrolyte was 513 mW·cm⁻² with R_p value of 0.3 Ω ·cm². The power output is nearly comparable to some other Co-based cathodes. In addition, the PBFZ-based cathode has lower TEC and is more compatible with the state-of-the-art protonic electrolytes. The structural features for fast oxygen ion diffusion, ease of oxygen vacancy formation, and the constant valence of dopant possibly contribute to the observed enhanced activity of PBFZ. These findings indicate that Zn doping remarkably improved the catalytic activity of the PBFZ cathode and increased the output performance of the single cell. The study indicates PBFZ is a promising material in

H-SOFCs as cathode at reduced temperatures and can open doors to propose new cathodes for BZCY-based cells.

Supplementary Materials: The following supporting information can be downloaded at: <https://www.mdpi.com/article/10.3390/catal12050488/s1>, Figure S1. The calculated thermal expansion coefficient; Figure S2. EIS plots of a symmetric PBF|SDC|PBF cell; Figure S3. I–V and I–P curves of PBF cathode based single-cell; Figure S4. (a) Impedance spectra for single cells, (b) calculated value of R_p , R_o , and R_t ; Figure S5. (a) SEM micrographs of the cell, (b) microstructure of PBF cathode; Figure S6. Energy Dispersive Spectrum (EDX) results.

Author Contributions: Conceptualization, B.L. and B.S.T.; methodology, B.S.T., B.A.B. and B.L.; validation, S.Z., K.K. and Y.C.; formal analysis, B.S.T. and B.A.B.; investigation, B.S.T., B.A.B. and B.L.; resources, B.L., D.T. and Y.C.; writing original draft preparation, B.S.T.; writing review and editing, B.L., K.K. and H.G.D.; supervision, B.L., D.T. and Y.C.; project administration, B.L.; funding acquisition, B.L., D.T. and Y.C. All authors have read and agreed to the published version of the manuscript.

Funding: This work was funded by the Fundamental Research Funds for the Central Universities of the University of Electronic Science and Technology of China (A03018023601020), the UESTCYDRI (U04210055), the Key Research and Development Project of Anhui Province (201904a07020002), the Anhui Provincial Department of Education (gxbjZD2021074), and the Huainan Science and Technology Bureau (2018A374) funded this research.

Data Availability Statement: Not applicable.

Acknowledgments: The authors wish to express their gratitude to the Huainan Normal University administration for providing facilities as well as thanks for the technical support of Quan Yang.

Conflicts of Interest: The authors declare no conflict of interest.

References

1. Xu, X.; Zhong, Y.; Shao, Z. Double Perovskites in Catalysis, Electrocatalysis, and Photo(electro)catalysis. *Trends Chem.* **2019**, *1*, 410–424. [[CrossRef](#)]
2. Zhang, Y.; Knibbe, R.; Sunarso, J.; Zhong, Y.; Zhou, W.; Shao, Z.; Zhu, Z. Recent Progress on Advanced Materials for Solid-Oxide Fuel Cells Operating Below 500 °C. *Adv. Mater.* **2017**, *29*, 1700132. [[CrossRef](#)] [[PubMed](#)]
3. Gao, Z.; Mogni, L.V.; Miller, E.C.; Railsback, J.G.; Barnett, S.A. A perspective on low-temperature solid oxide fuel cells. *Energy Environ. Sci.* **2016**, *9*, 1602–1644. [[CrossRef](#)]
4. Boldrin, P.; Ruiz-Trejo, E.; Mermelstein, J.; Menéndez, J.M.B.; Reina, T.R.; Brandon, N.P. Strategies for Carbon and Sulfur Tolerant Solid Oxide Fuel Cell Materials, Incorporating Lessons from Heterogeneous Catalysis. *Chem. Rev.* **2016**, *116*, 13633–13684. [[CrossRef](#)] [[PubMed](#)]
5. Kim, J.H.; Manthiram, A. Layered LnBaCo₂O_{5+δ} Perovskite Cathodes for Solid Oxide Fuel Cells: An Overview and Perspective. *J. Mater. Chem. A* **2015**, *3*, 24195–24210. [[CrossRef](#)]
6. Choi, S.; Kucharczyk, C.J.; Liang, Y.; Zhang, X.; Takeuchi, I.; Ji, H.-I.; Haile, S.M. Exceptional power density and stability at intermediate temperatures in protonic ceramic fuel cells. *Nat. Energy* **2018**, *3*, 202–210. [[CrossRef](#)]
7. Xu, X.; Wang, H.; Ma, J.; Liu, W.; Wang, X.; Fronzi, M.; Bi, L. Impressive performance of proton-conducting solid oxide fuel cells using a first-generation cathode with tailored cations. *J. Mater. Chem. A* **2019**, *7*, 18792–18798. [[CrossRef](#)]
8. Xia, Y.; Jin, Z.; Wang, H.; Gong, Z.; Lv, H.; Peng, R.; Liu, W.; Bi, L. A novel cobalt-free cathode with triple-conduction for proton-conducting solid oxide fuel cells with unprecedented performance. *J. Mater. Chem. A* **2019**, *7*, 16136–16148. [[CrossRef](#)]
9. Fabbri, E.; Pergolesi, D.; Traversa, E. Materials challenges toward proton-conducting oxide fuel cells: A critical review. *Chem. Soc. Rev.* **2010**, *39*, 4355–4369. [[CrossRef](#)] [[PubMed](#)]
10. Meng, Y.; Gao, J.; Zhao, Z.; Amoroso, J.; Tong, J.; Brinkman, K.S. Review: Recent progress in low-temperature proton-conducting ceramics. *J. Mater. Sci.* **2019**, *54*, 9291–9312. [[CrossRef](#)]
11. Zhou, C.; Sunarso, J.; Song, Y.; Dai, J.; Zhang, J.; Gu, B.; Zhou, W.; Shao, Z. New reduced-temperature ceramic fuel cells with dual-ion conducting electrolyte and triple-conducting double perovskite cathode. *J. Mater. Chem. A* **2019**, *7*, 13265–13274. [[CrossRef](#)]
12. Kim, J.; Sengodan, S.; Kwon, G.; Ding, D.; Shin, J.; Liu, M.; Kim, G. Triple-Conducting Layered Perovskites as Cathode Materials for Proton-Conducting Solid Oxide Fuel Cells. *ChemSusChem* **2014**, *7*, 2811–2815. [[CrossRef](#)] [[PubMed](#)]
13. Ren, R.; Wang, Z.; Meng, X.; Xu, C.; Qiao, J.; Sun, W.; Sun, K. Boosting the Electrochemical Performance of Fe-Based Layered Double Perovskite Cathodes by Zn²⁺ Doping for Solid Oxide Fuel Cells. *ACS Appl. Mater. Interfaces* **2020**, *12*, 23959–23967. [[CrossRef](#)] [[PubMed](#)]

14. Choi, S.; Shin, J.; Kim, G. The electrochemical and thermodynamic characterization of $\text{PrBaCo}_{2-x}\text{Fe}_x\text{O}_{5+\delta}$ ($x = 0, 0.5, 1$) infiltrated into yttria-stabilized zirconia scaffold as cathodes for solid oxide fuel cells. *J. Power Sources* **2012**, *201*, 10–17. [[CrossRef](#)]
15. Kim, G.; Wang, S.; Jacobson, A.J.; Reimus, L.; Brodersen, P.; Mims, C.A. Rapid oxygen ion diffusion and surface exchange kinetics in $\text{PrBaCo}_2\text{O}_{5+\delta}$ with a perovskite related structure and ordered A cations. *J. Mater. Chem.* **2007**, *17*, 2500–2505. [[CrossRef](#)]
16. Ding, H.; Xue, X.; Liu, X.; Meng, G. A novel layered perovskite cathode for proton conducting solid oxide fuel cells. *J. Power Sources* **2010**, *195*, 775–778. [[CrossRef](#)]
17. Zhao, L.; He, B.; Lin, B.; Ding, H.; Wang, S.; Ling, Y.; Peng, R.; Meng, G.; Liu, X. High performance of proton-conducting solid oxide fuel cell with a layered $\text{PrBaCo}_2\text{O}_{5+\delta}$ cathode. *J. Power Sources* **2009**, *194*, 835–837. [[CrossRef](#)]
18. Grimaud, A.; Bassat, J.-M.; Mauvy, F.; Pollet, M.; Wattiaux, A.; Marrony, M.; Grenier, J.-C. Oxygen reduction reaction of $\text{PrBaCo}_{2-x}\text{Fe}_x\text{O}_{5+\delta}$ compounds as H^+ -SOFC cathodes: Correlation with physical properties. *J. Mater. Chem. A* **2014**, *2*, 3594–3604. [[CrossRef](#)]
19. Chen, D.; Wang, F.; Shi, H.; Ran, R.; Shao, Z. Systematic evaluation of Co-free $\text{LnBaFe}_2\text{O}_{5+\delta}$ (Ln=Lanthanides or Y) oxides towards the application as cathodes for intermediate-temperature solid oxide fuel cells. *Electrochim. Acta* **2012**, *78*, 466–474. [[CrossRef](#)]
20. Yang, Z.; Ding, Z.; Xiao, J.; Zhang, H.; Ma, G.; Zhou, Z. A novel cobalt-free layered perovskite-type $\text{GdBaFeNiO}_{5+\delta}$ cathode material for proton-conducting intermediate temperature solid oxide fuel cells. *J. Power Sources* **2012**, *220*, 15–19. [[CrossRef](#)]
21. Zhao, F.; Wang, S.; Brinkman, K.; Chen, F. Layered perovskite $\text{PrBa}_{0.5}\text{Sr}_{0.5}\text{Co}_2\text{O}_{5+\delta}$ as high-performance cathode for solid oxide fuel cells using oxide proton-conducting electrolyte. *J. Power Sources* **2010**, *195*, 5468–5473. [[CrossRef](#)]
22. Mao, X.; Wang, W.; Ma, G. A novel cobalt-free double-perovskite $\text{NdBaFe}_{1.9}\text{Nb}_{0.1}\text{O}_{5+\delta}$ cathode material for proton-conducting IT-SOFC. *Ceram. Int.* **2015**, *41*, 10276–10280. [[CrossRef](#)]
23. Ding, H.; Xue, X. $\text{BaZr}_{0.1}\text{Ce}_{0.7}\text{Y}_{0.1}\text{Yb}_{0.1}\text{O}_{3-\delta}$ electrolyte-based solid oxide fuel cells with cobalt-free $\text{PrBaFe}_2\text{O}_{5+\delta}$ layered perovskite cathode. *J. Power Sources* **2010**, *195*, 7038–7041. [[CrossRef](#)]
24. Kim, D.; Son, S.J.; Kim, M.; Park, H.J.; Joo, J.H. $\text{PrBaFe}_2\text{O}_{5+\delta}$ Promising Electrode for Redox-Stable Symmetrical Proton-Conducting Solid Oxide Fuel Cells. *J. Eur. Ceram. Soc.* **2021**, *41*, 5939–5946. [[CrossRef](#)]
25. Li, F.; Tao, Z.; Dai, H.; Xi, X.; Ding, H. A high-performing proton-conducting solid oxide fuel cell with layered perovskite cathode in intermediate temperatures. *Int. J. Hydrogen Energy* **2018**, *43*, 19757–19762. [[CrossRef](#)]
26. Ding, H.; Xue, X. Novel Layered Perovskite $\text{GdBaCoFeO}_{5+\delta}$ as a Potential Cathode for Proton-Conducting Solid Oxide Fuel Cells. *Int. J. Hydrogen Energy* **2010**, *35*, 4311–4315. [[CrossRef](#)]
27. Ren, R.; Wang, Z.; Meng, X.; Wang, X.; Xu, C.; Qiao, J.; Sun, W.; Sun, K. Tailoring the Oxygen Vacancy to Achieve Fast Intrinsic Proton Transport in a Perovskite Cathode for Protonic Ceramic Fuel Cells. *ACS Appl. Energy Mater.* **2020**, *3*, 4914–4922. [[CrossRef](#)]
28. Hashim, S.S.; Liang, F.; Zhou, W.; Sunarso, J. Cobalt-Free Perovskite Cathodes for Solid Oxide Fuel Cells. *ChemElectroChem* **2019**, *6*, 3549–3569. [[CrossRef](#)]
29. Ding, H.; Xie, Y.; Xue, X. Electrochemical performance of $\text{BaZr}_{0.1}\text{Ce}_{0.7}\text{Y}_{0.1}\text{Yb}_{0.1}\text{O}_{3-\delta}$ electrolyte-based proton-conducting SOFC solid oxide fuel cell with layered perovskite $\text{PrBaCo}_2\text{O}_{5+\delta}$ cathode. *J. Power Sources* **2011**, *196*, 2602–2607. [[CrossRef](#)]
30. Xia, Y.; Xu, X.; Teng, Y.; Lv, H.; Jin, Z.; Wang, D.; Peng, R.; Liu, W. A novel $\text{BaFe}_{0.8}\text{Zn}_{0.1}\text{Bi}_{0.1}\text{O}_{3-\delta}$ cathode for proton conducting solid oxide fuel cells. *Ceram. Int.* **2020**, *46*, 25453–25459. [[CrossRef](#)]
31. Zohourian, R.; Merkle, R.; Raimondi, G.; Maier, J. Mixed-Conducting Perovskites as Cathode Materials for Protonic Ceramic Fuel Cells: Understanding the Trends in Proton Uptake. *Adv. Funct. Mater.* **2018**, *28*, 1801241. [[CrossRef](#)]
32. Chen, G.; Sunarso, J.; Wang, Y.; Ge, C.; Yang, J.; Liang, F. Evaluation of A-site deficient $\text{Sr}_{1-x}\text{Sc}_{0.175}\text{Nb}_{0.025}\text{Co}_{0.8}\text{O}_{3-\delta}$ ($x=0, 0.02, 0.05$ and 0.1) perovskite cathodes for intermediate-temperature solid oxide fuel cells. *Ceram. Int.* **2016**, *42*, 12894–12900. [[CrossRef](#)]
33. Wei, B.; Lü, Z.; Huang, X.; Liu, M.; Li, N.; Su, W. Synthesis, electrical and electrochemical properties of $\text{Ba}_{0.5}\text{Sr}_{0.5}\text{Zn}_{0.2}\text{Fe}_{0.8}\text{O}_{3-\delta}$ perovskite oxide for IT-SOFC cathode. *J. Power Sources* **2008**, *176*, 1–8. [[CrossRef](#)]
34. Jun, A.; Yoo, S.; Ju, Y.-W.; Hyodo, J.; Choi, S.; Jeong, H.Y.; Shin, J.; Ishihara, T.; Lim, T.-H.; Kim, G. Correlation between fast oxygen kinetics and enhanced performance in Fe doped layered perovskite cathodes for solid oxide fuel cells. *J. Mater. Chem. A* **2015**, *3*, 15082–15090. [[CrossRef](#)]
35. Li, P.; Yang, Q.; Zhang, H.; Yao, M.; Yan, F.; Fu, D. Effect of Fe, Ni and Zn dopants in $\text{La}_{0.9}\text{Sr}_{0.1}\text{CoO}_{3-\delta}$ on the electrochemical performance of single-component solid oxide fuel cell. *Int. J. Hydrogen Energy* **2020**, *45*, 11802–11813. [[CrossRef](#)]
36. Wang, Z.; Lv, P.; Yang, L.; Guan, R.; Jiang, J.; Jin, F.; He, T. $\text{Ba}_{0.95}\text{La}_{0.05}\text{Fe}_{0.8}\text{Zn}_{0.2}\text{O}_{3-\delta}$ cobalt-free perovskite as a triple-conducting cathode for proton-conducting solid oxide fuel cells. *Ceram. Int.* **2020**, *46*, 18216–18223. [[CrossRef](#)]
37. Priya, N.S.C.; Sandhya, K.; Rajendran, D.N. Study on Electrical conductivity and Activation Energy of doped Ceria nanostructures. *Electrochem. Energy Technol.* **2018**, *3*, 49–53. [[CrossRef](#)]
38. M'Peko, J.-C.; Ruiz-Salvador, A.R.; Rodríguez-Fuentes, G. Conductivity activation energy and analysis of the sintering process of dielectric ceramics. *Mater. Lett.* **1998**, *36*, 290–293. [[CrossRef](#)]
39. Chen, T.; Pang, S.; Shen, X.; Jiang, X.; Wang, W. Evaluation of Ba-deficient $\text{PrBa}_{1-x}\text{Fe}_2\text{O}_{5+\delta}$ oxides as cathode materials for intermediate-temperature solid oxide fuel cells. *RSC Adv.* **2016**, *6*, 13829–13836. [[CrossRef](#)]
40. Cai, B.; Song, T.-F.; Su, J.-R.; He, H.; Liu, Y. Comparison of (Pr, Ba, Sr) $\text{FeO}_{3-\delta}$ -SDC composite cathodes in proton-conducting solid oxide fuel cells. *Solid State Ionics* **2020**, *353*, 115379. [[CrossRef](#)]
41. Liu, B.; Yang, J.; Yan, D.; Jia, L.; Chi, B.; Pu, J.; Li, J. Novel $\text{PrBa}_{0.9}\text{Ca}_{0.1}\text{Co}_{2-x}\text{Zn}_x\text{O}_{5+\delta}$ double-perovskite as an active cathode material for high-performance proton-conducting solid oxide fuel cells. *Int. J. Hydrogen Energy* **2020**, *45*, 31009–31016. [[CrossRef](#)]

42. Jin, F.; Xu, H.; Long, W.; Shen, Y.; He, T. Characterization and Evaluation of Double Perovskites $\text{LnBaCoFeO}_{5+\delta}$ (Ln = Pr and Nd) as Intermediate-Temperature Solid Oxide Fuel Cell Cathodes. *J. Power Sources* **2013**, *243*, 10–18. [[CrossRef](#)]
43. Xia, W.; Liu, X.; Jin, F.; Jia, X.; Shen, Y.; Li, J. Evaluation of calcium codoping in double perovskite $\text{PrBaCo}_2\text{O}_{5+\delta}$ as cathode material for IT-SOFCs. *Electrochim. Acta* **2020**, *364*, 137274. [[CrossRef](#)]
44. Ling, Y.; Lin, B.; Zhao, L.; Zhang, X.; Yu, J.; Peng, R.; Meng, G.; Liu, X. Layered perovskite $\text{LaBaCuMO}_{5+\delta}$ (M = Fe, Co) cathodes for intermediate-temperature protonic ceramic membrane fuel cells. *J. Alloy. Compd.* **2010**, *493*, 252–255. [[CrossRef](#)]
45. Zhao, L.; He, B.; Xun, Z.; Wang, H.; Peng, R.; Meng, G.; Liu, X. Characterization and evaluation of $\text{NdBaCo}_2\text{O}_{5+\delta}$ cathode for proton-conducting solid oxide fuel cells. *Int. J. Hydrogen Energy* **2010**, *35*, 753–756. [[CrossRef](#)]